Study on the Flow Structure inside Subchannels of 4×6 Rod-bundle Array

Seok Kim [a*], Hae-Seob Choi[a], Byong Gook Jeon [a], Sang-Ki Moon[a]
[a]*Thermal Hydraulics Safety Research Division, Korea Atomic Energy Research Institute*
111 Daedeok-daero989beongil, Yuseong-gu, Daejeon, 34057, Republic of Korea
[*]*Corresponding author: seokim@kaeri.re.kr*

1. Introduction

The fuel rod-bundle assembly in a PWR (Pressurized Water Reactor) belongs to the class of square-latticed vertical rod-bundle geometries. In square-latticed geometry, the flow area, surrounded by four rods, defines a subchannel. Each subchannel connects to adjacent ones by a gap between two rods. The major axial flow direction is vertical, but there is also a transverse flow between two adjacent subchannels through the gaps, known as crossflow. Rowe et al. [1] showed that macroscopic flow structures exist adjacent to the gap region in a square-arrayed rod-bundle geometry. Furthermore, they found that rod gap spacing (P/D) is the most significant geometric parameter affecting flow structure. It is clear from previous studies that single-phase turbulent large-scale coherent vortices are the main contributor to the crossflow mixing. Because large-scale coherent vortices in a rod-bundle affect the flow characteristics inside a subchannel, quantification of contribution to the crossflow mixing is needed, along with the importance of analyzing the flow structure inside the rod-bundle. Noble research works on the flow structure inside the subchannel of rod-bundle was carried out by several researchers. McClusky et al. [2] studied the development of swirling flow in a 5×5 rod-bundle by using particle image velocimetry (PIV) technique. Chang et al. [3] performed 2D laser-Doppler anemometry (LDA) measurements in a 5 ×5 fuel rod-bundle with two types of spacer grids. The velocity measurement researches were performed by using an optically transparent experimental facility, but there were some limitations the flow measurements in the inaccessible areas of rod-bundle. The matched index-of-refraction (MIR) technique is the most effective method to allow laser diagnostic techniques such as PIV and LDA. Dominguez-Ontiveros et al. [4] presented their velocity measurements by using time-resolved PIV technique in a 5×5 fuel rod-bundle. However, most of the existing studies were conducted by distorting the hydraulic diameter or pitch-to-diameter of the actual nuclear fuel assembly for convenience for visualization experiment. There is a possibility that errors may occur when applied to the nuclear safety analysis by distorted geometric characteristics. In this study, we tried to preserve the geometrical figures of the fuel rod array and accumulate experimental database to identify the crossflow or mixing characteristics between the fuel assemblies.

2. Test Facility

Figure 1 shows a schematic of the experiment facility called PRIUS-I. The fluid system consists of a test section, a storage tank, and a 2-inch piping system for the water supply to the test section and return back to the storage tank. The storage tank is installed at the top of the facility and is opened normally. The water temperature in the system is controlled using a cooler and heater imbedded in the storage tank. The water flow is supplied using a centrifugal pump with a 40 m head and 48 m^3/hr capacity, which is controlled by adjusting the impeller speed using an inverter. The maximum achievable Reynolds number based on the hydraulic diameter in the PRIUS-I test facility is approximately 70,000. The range of Reynolds numbers that the PRIUS-I can simulate corresponds to the Reynolds number covering a SB/IB-LOCA accident condition [5]. A bypass line is established at the upstream of the test section for efficient control of the water flowrate. In the piping line, which is divided into two branch lines, instrumentations for the flow rate, temperature, and pressure are installed. To maintain a straight flow at the inlet, a multi-hole plate and honeycomb is installed inside the tranquillization chamber.

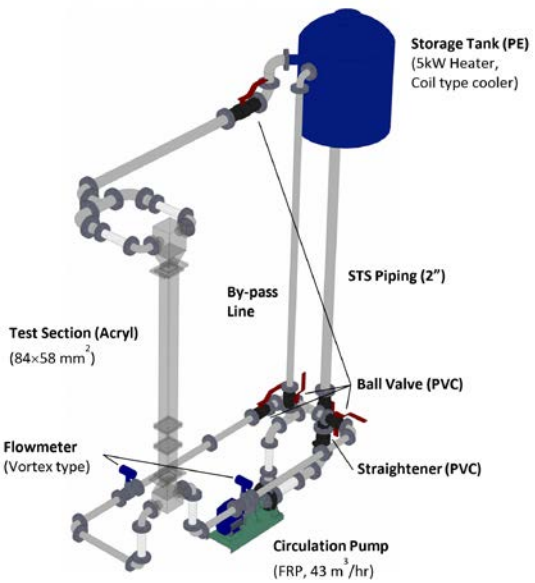

Fig. 1. Schematic of the test facility (PRIUS-I).

Figure 2 shows a detailed geometrical dimensions of PRIUS-I test section. The PRIUS test section has rectangular geometry with dimensions of 84 mm × 58

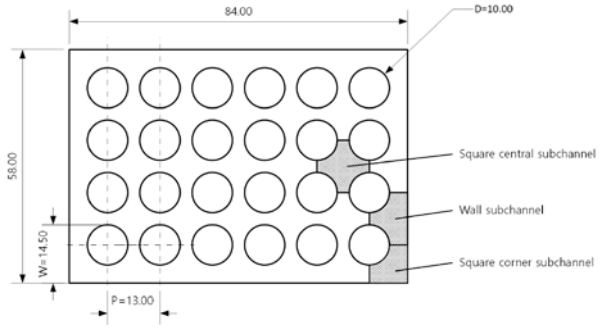

Fig. 2. Geometry of 4 × 6 rod bundles.

mm × 1.5 m, and this is made of 15-mm-thick acryl. In the PRIUS-I experiment, the design of the rod array focuses on a small-sized rod-bundle test to establish the MIR-PIV measurement methodology and provide sufficient subchannel crossflow and mixing caused in a small-sized test facility. Furthermore, preliminary CFD calculations show that flow in a 4×6 rod-bundle model would provide sufficiently high Reynolds numbers for fully turbulent flow. To remove the image distortion induced by the different refraction indexes of water and acryl rods, the MIR technique [6] has been adopted. Practical optical flow measurements in a rod-bundle geometry would be impossible without MIR. The merit of the MIR technique is that it permits the optical measurement to identify flow characteristics inside the subchannels and gap between adjacent rods without distortion of the optical paths. The working fluid is chosen in combination with a solution of 62.5% sodium iodide (NaI) in 37.5% demineralized water of 30 °C. The viscosity of the NaI solution is low enough to enable Reynolds-number identity with a feasible mass flow. The working fluid temperature is maintained using a temperature control system. A heat exchanger with a capacity of 10 kW and an electrical heater with a capacity of 5 kW are installed in the PRIUS-I test facility. The temperature control system can maintain the working fluid temperature in the PRIUS-I test loop within ± 0.1 °C of the specified index-matching temperature. The refractive index of acryl is about 1.49 at 30 °C. The refractive index of the NaI working fluid is measured by a digital refractometer (KRUSS Co., DR6200-T). The density and dynamic viscosity of the NaI working fluid is also measured by the force tensiometer (KRUSS Co., K20) and the rheometer (Brookfield Co., DV3T), respectively. Because the NaI solution is highly corrosive to ferrous metals, even to stainless steels, piping with Teflon coating for preventing corrosion has been installed. The internals of the circular pump are made of FRP (fiber-reinforced plastic). The valves and the storage tank are also made of PVC (polyvinyl chloride) or PE (polyethylene).

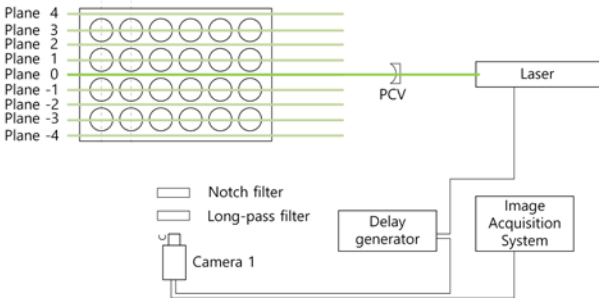

Fig. 3. Experimental setup of PIV measurement system.

3. Experimental Set-up

Figure 3 shows a schematic diagram of the optical setup for PIV velocity field measurements, consisting of a 65-mJ Nd:YAG laser with an emission wavelength of 532 nm, a 2K × 2K CCD (Charged-Coupled Device) camera, and a delay generator. The acquisition rate of the raw image is controlled by a delay generator, and in this study, five frames per second were used. The laser light sheet illuminated the test flow from the right, as shown in Figure 3. A fluorescent polymer bead coated with Rhodamine B, having an average diameter of 20 μm and a specific gravity of 1.02, was used as the tracer particles. A long pass filter (λ > 550 nm) and a notch filter were used to eliminate the scattered light, except the fluorescence light, and block the 532 nm wavelength light. These were installed in front of the CCD camera. Using the ensemble average of 1,000 instantaneous velocity vector fields, statistical results could be obtained, such as the mean velocity vector fields and turbulence intensity. The velocity fields for interrogation window size of 64 × 64 pixel^2 calculated with 50% overlap were used for the final interrogation window size of 32 × 32 pixel^2. This results in an effective spatial resolution of 16 × 16 pixel^2. After the calibration of the images, a resolution of 41 × 41 μm^2/pixel was achieved. This corresponds to an effective spatial resolution of 0.66 × 0.66 mm^2 for the final velocity field. Table 1 shows a test matrix for the visualization experiment. For the PIV measurement, experiments were performed on three kinds of Reynolds number with two inlet flow conditions. By the ensemble average of 1,000 instantaneous velocity vector fields, the statistical results of the mean velocity vector fields, turbulence intensity, and turbulent kinetic energy could be obtained.

Table 1: Test matrix of PRIUS-I.

V_{left}/V_{total}	Re(total)		
	10000	20000	30000
0.5	⊕	⊕	⊕
0.7	⊕	⊕	⊕

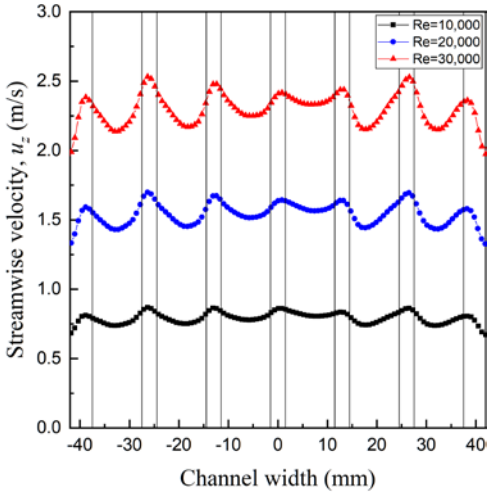

(a) Uniform inlet condition

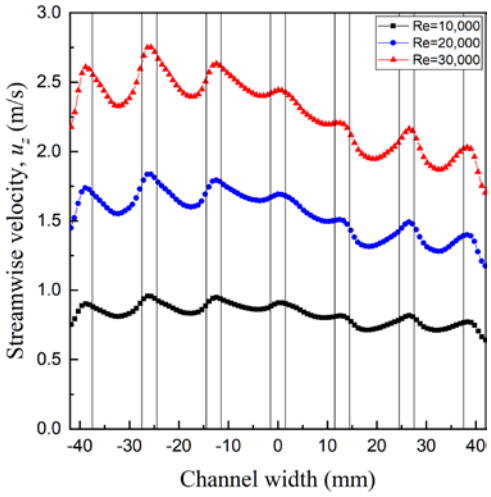

(b) Non-uniform inlet condition

Fig. 4. Streamwise mean velocity profiles at the center section (plane 0).

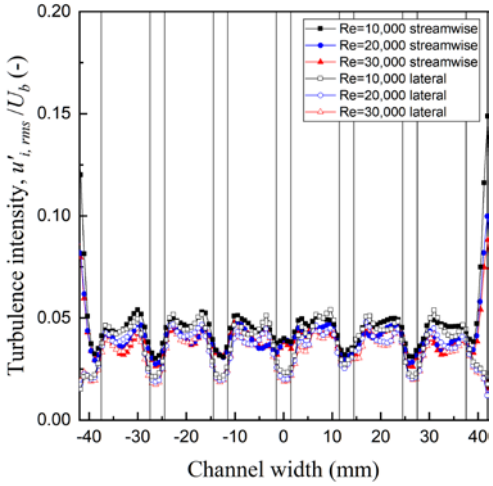

(a) Uniform inlet condition

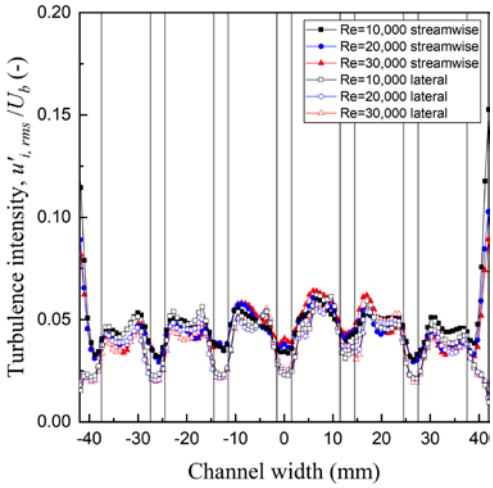

(b) Non-uniform inlet condition

Fig. 5. Streamwise and lateral turbulence intensity profiles at the center section (plane 0).

4. Results and Discussions

Figure 4 and Figure 5 show the streamwise mean velocity and the streamwise/lateral turbulence intensity at the center section according to the flow conditions from Re=10,000 to 30,000, respectively. The streamwise velocity profile along the channel width clearly identifies the flow in the gap region and the region behind the rod. The asymmetrical behavior of the mean velocity and turbulence intensity profile along the channel width is due to the non-uniform inlet velocity condition. The turbulence intensity profiles shows the periodic shape with a pitch (*P*). The turbulence intensity in the gap is much higher than that in the subchannel center due to the mixing. The streamwise turbulence intensity is gradually decreased toward the wall and increases sharply near the wall. The lateral turbulence intensity has a tendency similar to the streamwise turbulent intensity except near the wall region.

The experimental data of the Re=20,000 condition based on hydraulic diameter were utilized to validate the prediction capability of the CFD code (STAR-CCM+ 11.02). The computation domain covered both the rod-bundle region and the upstream inlet regions. In mesh generation, over six million polyhedral cells were used, and a mesh sensitivity study was conducted in advance. The minimum cell thickness was about 0.2 mm at the rod surface. The steady solution was obtained by monitoring velocity histories at different locations. We used the workstation with 116 cores. The implicit unsteady calculation was conducted using 3-D incompressible isothermal flow, Menter's k-ω SST (Shear Stress Transport) turbulence model with all y+ wall treatment, realizable k-ε model with all y+ wall treatment, and RST (Reynolds Stress Transport) model with linear pressure strain model (standard and two layer). The k-ω and k-ε models require less computational cost because they solve two equations to calculate a turbulent viscosity. On the other hand, the RST model is more accurate and takes more time because it solves seven equations for each component of the Reynolds stress tensor. Regarding the boundary conditions, mass flow boundary conditions were imposed using measured flow rates at the inlet regions

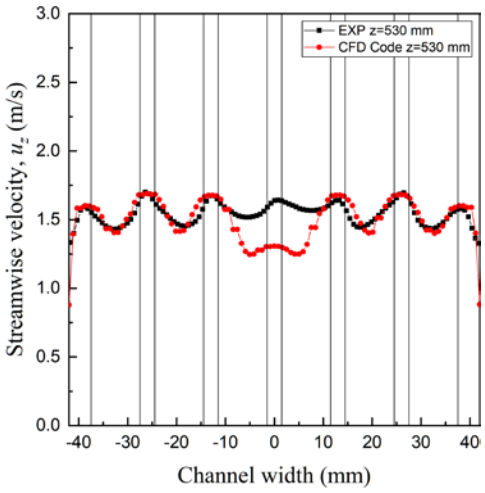

(a) Uniform inlet condition

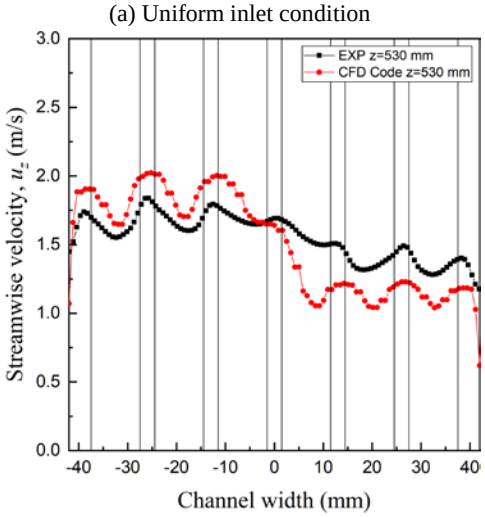

(b) Non-uniform inlet condition

Fig. 6. Streamwise mean velocity profile compared with CFD analysis results at the center plane (Re=20,000).

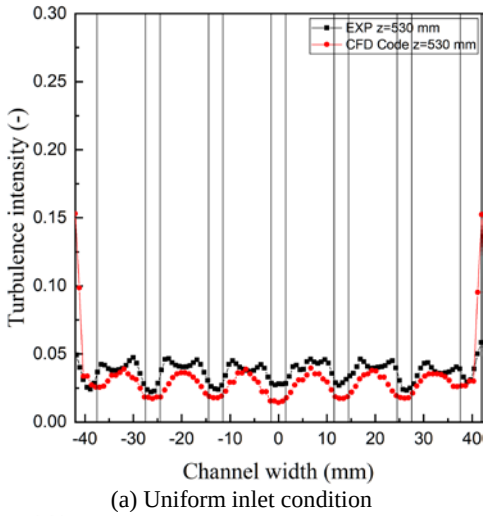

(a) Uniform inlet condition

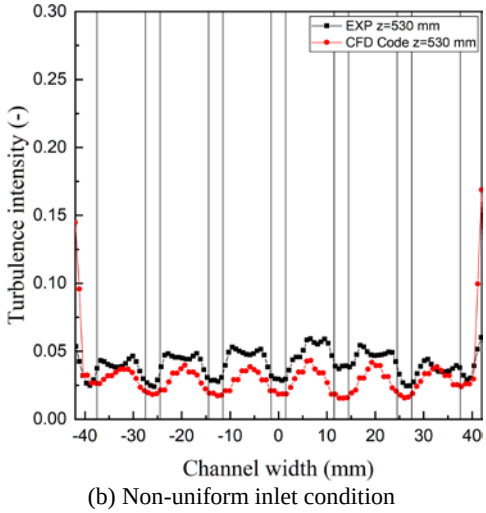

(b) Non-uniform inlet condition

Fig. 7. Turbulence intensity profile compared with CFD analysis results at the center plane (Re=20,000).

and the pressure outlet boundary was imposed at the downstream of the rod-bundle region. Material properties for the working fluid at 30°C were used. The representative comparison results were given by the realizable k-ε model with all y+ wall treatment. Figure 6 shows the streamwise velocity profile along the center plane at 530 mm downstream from the inlet of the test section. Figure 6 (left) shows the uniform inlet flow condition, which has a symmetric velocity profile. Apart from the center region (i.e., width < 5 mm), the overall trend was reproduced for the case of the uniform inlet velocity condition. Figure 6 (right) shows the non-uniform inlet flow condition, which has the higher velocity at the left region. In the CFD code calculation, flow was not mixed efficiently compared with the experimental results. Figure 7 shows the turbulence intensity at the same location as Figure 6. For both uniform and non-uniform inlet flow conditions, the turbulence intensity was under-predicted. This lower turbulence intensity in the calculation can lead to less mixing in the non-uniform inlet flow condition. Figure 8 shows the turbulent model sensitivity for the case of Re=20,000 at plane 0 under the non-uniform inlet velocity condition. The difference of calculation results according to the different turbulence models is small, but the SST k-ω turbulence model and the RST model show the best agreement with the experimental results. By examining different turbulence models and modifying the constituting parameters, the underlying physics will be explored further. The experimental results are expected to be used in the verification of the subchannel analysis codes because it includes information about the lateral flow velocity distributions in gaps between adjacent subchannels.

5. Conclusions

The PRIUS-I experiment has addressed many important topics related to flow behaviour in a rod-bundle. These issues relate to the flow conditions inside a nuclear fuel element during the normal plant operation or in accident scenarios. Flow visualization has been performed using a MIR-PIV technique, from which

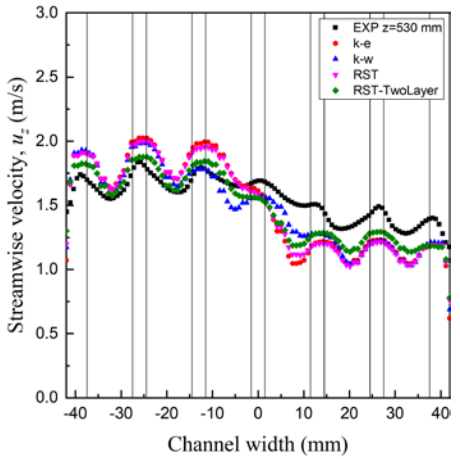

(a) Streamwise mean velocity

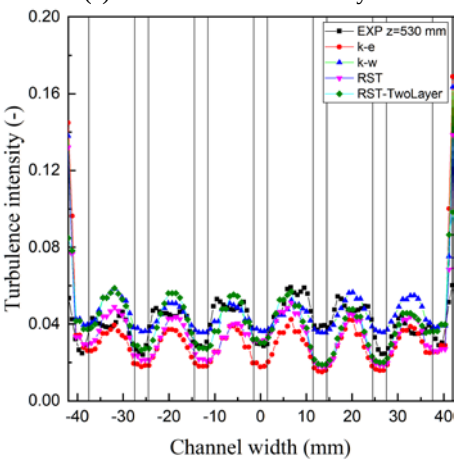

(b) Turbulence intensity

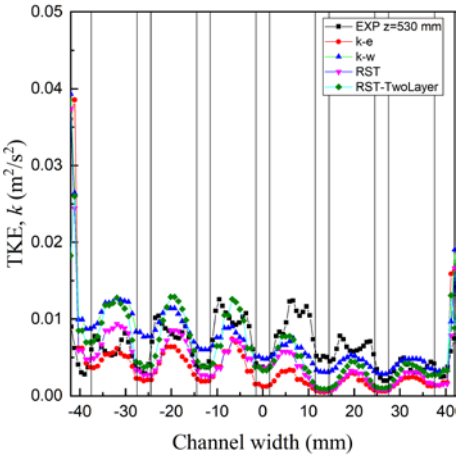

(c) Turbulent kinetic energy

Fig. 8. Comparison of turbulent model at plane 0 under the non-uniform inlet velocity condition (Re=20,000).

detailed information for the two-dimensional movement of single-phase flow has been quantified and compared with CFD analysis results. In particular, the visualization results using the MIR technique have shown that any section of the rod-bundle geometry can be visualized. The experimental database in a rod-bundle geometry will address the modelling and validation of subchannel analysis. It can also be useful for CFD in open medium validation. As a further work, the PRIUS-II test program to build the experimental database for nuclear fuel assembly scale will be under way by 2020. The typical configuration for the rod-bundle will consist of 8×24 unheated rods representing three ¼-scaled PWR fuel assemblies.

ACKNOWLEDGMENTS

This work was supported by the National Research Foundation of Korea (NRF) grant funded by the Korea government (MSIP) (No. 2012M2A8A4004176 and 2017M2A8A4015026).

REFERENCES

[1] Rowe, D. S., Johnson, B. M., Knudsen, J. G., “Implications Concerning Rod Bundle Crossflow Mixing based on Measurements of Turbulent Flow Structure”, Int. J. Heat Mass Transfer, Vol. 17, pp. 407-419 (1974)

[2] McClusky, H.L., Holloway, M.V., Beasley, D.E. and Conner, M.E., “Development of swirling flow in a rod bundle subchannel”, Journal of Fluids Engineering, Vol. 124, (2002)

[3] Chang, S.-K., Kim, S., Song, C.-H., “Turbulent mixing in a rod bundle with vaned spacer grids: OECD/NEA–KAERI CFD benchmark exercise test”, Nuclear Engineering and Design, Vol. 279, pp. 19–36 (2014)

[4] Dominguez-Ontiveros, E.E., Hassan, Y.A., “Non-intrusive experimental investigation of flow behavior inside a 5 ×5 rod bundle with spacer grids using PIV and MIR”, Nuclear Engineering and Design, Vol. 239, pp. 888–898 (2009)

[5] D. Bestion, M. Valette, P. Fillion, P. Gaillard, 3D Core thermalhydraulic phenomena in PWR SBLOCAs and IBLOCAs, NURETH-17, Sept 2017, Xian, China

[6] Stoots, C.M., Becker, S., Condie, K.G., Durst, F. and McEligot, D.M., “A Large-Scale Matched-Index-Of Refraction Flow Facility For LDA Studies Of Complex Geometries”, Exp. Fluids, Vol. 30, pp. 391-398 (2001)